

# Substructure of Clusters of Galaxies and Cosmological Constant

Tamon Suwa and Asao Habe

*Division of Physics, Graduate School of Science, Hokkaido University, Sapporo 060-0810,  
Japan*

[tamon@astro1.sci.hokudai.ac.jp](mailto:tamon@astro1.sci.hokudai.ac.jp)

[habe@astro1.sci.hokudai.ac.jp](mailto:habe@astro1.sci.hokudai.ac.jp)

Kohji Yoshikawa

*Department of Astronomy, Kyoto University, Kyoto 606-8502, Japan*

[kohji@kusastro.kyoto-u.ac.jp](mailto:kohji@kusastro.kyoto-u.ac.jp)

and

Takashi Okamoto

*Yukawa Institute for Theoretical Physics, Kyoto University, Kyoto 606-8502, Japan*

[tokamoto@yukawa.kyoto-u.ac.jp](mailto:tokamoto@yukawa.kyoto-u.ac.jp)

## ABSTRACT

We investigate possibility of utilizing substructures in clusters of galaxies as a probe of the non-zero cosmological constant,  $\Lambda$ . Using high-resolution cosmological N-body/SPH simulations of flat ( $\Omega_0 = 0.3$ ,  $\lambda_0 = 0.7$ ,  $\Lambda$ CDM) and open ( $\Omega_0 = 0.3$ ,  $\lambda_0 = 0$ , OCDM) cold dark matter dominated universes, we obtain indicators that are closely related with the substructures from each cosmological model. As the indicators, we calculate axial ratios, center shifts, cluster clumpiness, and multipole moment power ratios for the simulated clusters at  $z = 0$  and 0.5. These indicators are calculated for both X-ray surface brightness and column density of the matter. In  $\Lambda$ CDM all these indicators tend to be larger than those in OCDM at  $z = 0$ . This result is consistent with the analytical prediction, that is, clusters in  $\Lambda$ CDM are formed later than in OCDM and then clusters in OCDM are more relaxed at  $z = 0$ . We make Kolmogorov-Smirnov test on each indicator. We then find that the results for the multipole moment power ratios and the center shifts for the X-ray surface brightness are under the significant level (5%) and we distinguish these two models more clearly at  $z = 0$  than  $z = 0.5$ .

*Subject headings:* galaxies:clusters:general – cosmology:theory – methods:numerical

## 1. INTRODUCTION

The quest for cosmological parameters, such as the Hubble constant  $H_0$ , the density parameter  $\Omega_0$ , and the cosmological constant  $\Lambda$ , is one of the most important problem in the observational cosmology. From observational evidences, the density parameter  $\Omega_0$  is estimated to be around 0.3 (e.g. Bahcall et al. 1999). The inflation cosmology requires  $\Omega_0 + \lambda_0 = 1$  that is supported by the recent observation of the cosmic microwave background (de Bernardis et al. 2000). Distant Type Ia supernovae (SNe Ia) are used to be cosmological candles to explore effect of the cosmological constant and evidence of the acceleration expansion (Perlmutter et al. 1999; Riess et al. 1998). However, several systematic uncertainties in the observational data of SNe Ia are pointed out (Totani & Kobayashi 1999; Gibson et al. 2000). Further studies are needed to confirm the presence of the cosmological constant. We study the effect of the cosmological constant on structures of galaxy clusters and what statistical indicator, which quantifies irregularity of the structure, is suitable to study it.

Richstone, Loeb, & Turner (1992) proposed that structures of clusters are closely related to a cosmological model, since the recently formed fraction of the clusters is strongly depends on a cosmological model. They showed that, in a denser universe, this fraction becomes larger. Several authors studied what indicator is suitable to show the effect of cosmological parameters in numerical simulations. Studied indicators are the axial ratio (Mohr et al. 1995; Jing et al. 1995; Thomas et al. 1998),  $M_{\text{int}}$  and  $M_{\text{ext}}$  (Thomas et al. 1998), the center shift (Jing et al. 1995; Thomas et al. 1998), the centroid variation (Mohr et al. 1995; Crone, Evrard, & Richstone 1996), the multipole moment power ratio (Buote & Tsai 1995, 1996; Tsai & Buote 1996; Buote & Xu 1997; Valdarnini, Ghissardi, & Bonometto 1999), and  $\Delta$ -statistic (Dutta 1995; Crone, Evrard, & Richstone 1996). These simulations have been performed in various cosmological models. In some of these studies they compared the results in cosmological models of different density parameters, including in the case of existence of cosmological constant (e.g. Crone, Evrard, & Richstone 1996; Buote & Xu 1997). They suggested the possibility of the application of the cluster substructures to distinguish the flat and open cold dark matter (CDM) models having the same density parameter.

These indicators have been mainly concerned with X-ray surface brightness of clusters of galaxies. At cluster formation epoch, gravitational potential energy is released and gas in the cluster is heated up to its virial temperature. Then heated gas emits X-ray. Hence, X-ray observation shows distribution of the hot gas in the cluster. On the other hand, gravitational potential of the cluster is dominated by the dark matter, then it is possible that column

density of total mass shows the total mass distribution which needs not to coincide with the gas distribution. Although the dark matter cannot be observed directly, a method by which the mass distribution is reconstructed from small distortions of background galaxies caused by gravitational lens (these small distortion is called ‘weak shear field’) is recently developed (e.g. Mellier 1999; Luppino & Kaiser 1997; Clowe et al. 2000). The precision of this method is not yet sufficient to prove the substructures of the clusters. It is, however, likely that this mass reconstruction method will progress and become a useful tool to measure substructures of galaxy cluster.

In this paper, we investigate the difference between  $\Lambda$ CDM and OCDM using the numerical simulations of clusters of galaxies in these models by Yoshikawa, Jing, & Suto (2000). We identify the clusters and calculate various statistical indicators. The Kolmogorov-Smirnov test (hereafter KS-test) is performed to measure how these indicators are effective to distinguish these two cosmological models. Our work is different from the previous studies on following points. (1) We use the data by the high resolution numerical simulations which includes not only dark matter particles but also gas particles. Some previous simulations (e.g. Jing et al. 1995; Buote & Xu 1997) used only N-body simulation. While other simulation (Mohr et al. 1995) employed gas particles, the number of the sample clusters obtained in the numerical results was small. (2) We focus on distinction between OCDM and  $\Lambda$ CDM here. While Valdarnini, Ghissardi, & Bonometto (1999) employed gas particles and the number of their simulated clusters were large enough to perform the statistical tests, they did not do simulation in OCDM. (3) We use two kinds of physical quantities, the X-ray surface brightness ( $\Sigma_X$ ) and the column density of the total mass ( $\sigma$ ), to calculate the statistical indicators, while the previous studies used only the X-ray surface brightness.

The organization of this paper is as follows. In §2, we describe the data used in this paper, cluster identification, and definitions of indicators we used. We derive the values of the indicators for simulated clusters and show results of the KS-test on them in §3. In §4, we discuss our results and present our conclusion.

## 2. METHOD

### 2.1. Simulation Data

Our simulations are based on particle-particle-particle-mesh ( $P^3M$ )-Smoothed Particle Hydrodynamics (SPH) algorithm (Yoshikawa, Jing, & Suto 2000). These simulations have sufficient resolution to research the substructure of the clusters and enough number of the clusters to perform statistical tests. We use two cosmological models, OCDM and  $\Lambda$ CDM.

Cosmological parameters, which are same for two models, except for the cosmological constant ( $\lambda_0$ ), are as follows: the Hubble constant in units of  $100 km\ s^{-1}\ Mpc^{-1}$ ,  $h = 0.7$ , the density parameter,  $\Omega_0 = 0.3$ , the baryon density parameter,  $\Omega_b = 0.015h^{-2}$ , the rms density fluctuation amplitude on a scale  $8h^{-1}Mpc$ ,  $\sigma_8 = 1.0$ , and the power-law index of the primordial density fluctuation,  $n = 1.0$ . The cosmological constant,  $\lambda_0$  is 0 (for OCDM) or 0.7 (for  $\Lambda$ CDM).

The simulation employs  $N_{DM} = 128^3$  dark matter particles and the same number of gas particles. Mass of dark matter and SPH particles are  $1.7 \times 10^{11} M_\odot$  and  $2.0 \times 10^{10} M_\odot$ , respectively. COSMICS package (Bertschinger 1995) is used to generate initial conditions at  $z = 25$ . Comoving size of simulation box,  $L_{\text{box}} = 150h^{-1}Mpc$ , and the box is on the periodic boundary condition.

We use the data at  $z = 0.5$  and 0 to calculate statistical indicators. The reason of this is that the formation rate of galaxy clusters in  $\Lambda$ CDM exceeds that in OCDM in  $z < 0.8$  as shown in Fig.1 which shows the formation rate of galaxy clusters as a function of redshift. The formation rate is differentiation of the number of formed clusters with respect to the cosmic time, where the number of formed clusters is normalized by the present value and the cosmic time is also normalized by the present age of universe. We obtain the formation rate in the similar way to Richstone, Loeb, & Turner (1992). The solid and dashed curves indicate the formation rates in  $\Lambda$ CDM and in OCDM, respectively. Since just before  $z = 0.5$  the formation rate in  $\Lambda$ CDM is over that in OCDM, we expect that the effect of difference of formation rate, i.e. the effect of cosmological constant, already appear at  $z = 0.5$ . Moreover, the mass reconstruction based on the observations of the weak shear field has an advantage for high-redshift clusters rather than nearby clusters in principle.

## 2.2. Cluster Identification

The way of identification of galaxy clusters is as follows (Jing & Fang 1994; Thomas et al. 1998).

1. Pick up SPH particles whose density is more than 200 times the background density.
2. Perform Friends-of-Friends method (e.g. Jing & Fang 1994). Linking length,  $l$ , is defined as  $b\bar{n}^{-1/3}$ , where  $\bar{n}$  is mean number density of SPH particles, and constant parameter  $b = 0.5$ . We find that the number of found clusters is not so different for  $0.2 < b < 10$ .
3. The densest SPH particle in each group is defined as a ‘core’ particle of the group.

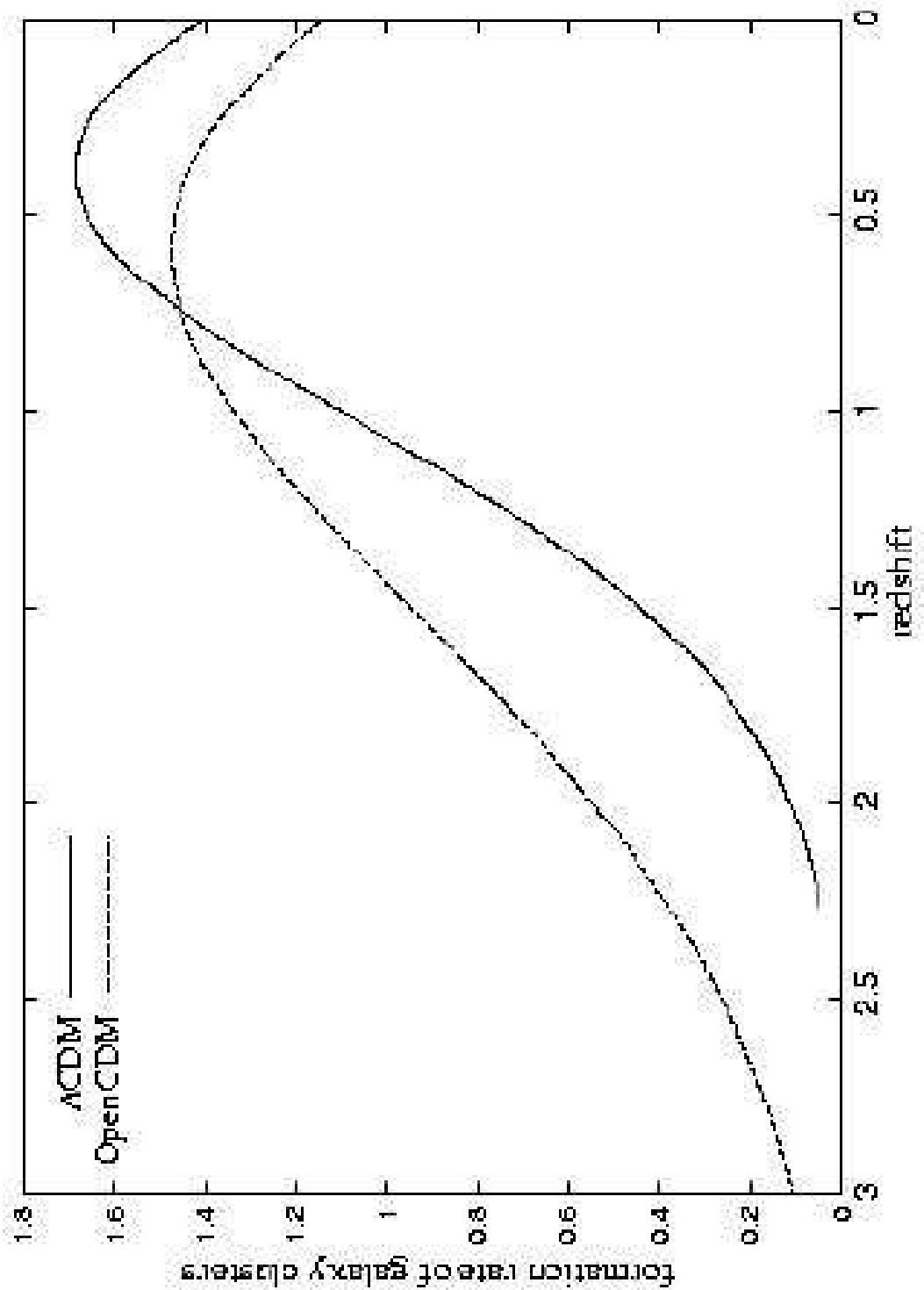


Fig. 1.— The formation rate of galaxy clusters. The solid curve indicates the formation rate in  $\Lambda$ CDM and the dashed curve indicate that in OCDM.

4. Draw sphere centered on the position of the ‘core’, and seek a radius in which mean density is 200 times the background density. This radius is called  $r_{200}$ .
5. If total mass of particles in the sphere with radius  $r_{200}$  is more than  $2 \times 10^{14}h^{-1}M_{\odot}$ , this set of particles in the sphere is a candidate of a cluster of galaxies.
6. If another ‘core’ particle exists in the sphere, the set which belongs to less dense ‘core’ is removed from the cluster candidate list.

The candidates which are not removed finally are identified as clusters of galaxies.

Table 1 shows numbers of clusters found in each model. The numbers of the clusters increase from  $z = 0.5$  to  $z = 0$ . Table 2 is the ratio of mass included clusters to total mass in the simulation box. These ratios in both models are similar to each other at  $z = 0$ , but the ratio in  $\Lambda$ CDM is smaller than that in OCDM at  $z = 0.5$ . This is consistent with the fact that  $\Lambda$ CDM clusters form later than OCDM clusters.

### 2.3. Projection to Two Dimension

Two of the indicators we use in this paper, the center shifts and the power ratios, are calculated for the X-ray surface brightness, and the column density of dark matter and gas in simulated clusters. Our numerical projection method from 3D to 2D is as follows.

At first, for each cluster, we assume a cube of which center is the center of the cluster with sides of  $2r_{200}$ . Total number of grid points in the cube is  $128^3$ . Each grid point is assigned by indices  $(i, j, k)$  and this point is expressed by  $\mathbf{r}_{ijk}$ . Then we calculate gas density and gas temperature at each grid point from SPH particles in this cube. Gas density,  $\rho$ , and gas temperature,  $T$ , at a grid point  $\mathbf{r}_{ijk}$  is given by

$$\rho(\mathbf{r}_{ijk}) = \sum_s W(r_{s;ijk}/h_s) \frac{m_s}{h_s^3}, \quad (1)$$

$$T(\mathbf{r}_{ijk}) = \sum_s \frac{(\gamma - 1)\mu m_p}{k_B} W(r_{s;ijk}/h_s) u_s, \quad (2)$$

Model	z=0	z=0.5
$\Lambda$ CDM	66	28
OCDM	74	38

Table 1: The number of the clusters for each model and redshift.

where  $h_s$ ,  $m_s$ ,  $u_s$ , and  $r_{s;ijk}$  are  $s$ -th particle's smoothing length, mass, specific energy, and distance to the grid point ( $r_{s;ijk} = |\mathbf{r}_{ijk} - \mathbf{r}_s|$ , where  $\mathbf{r}_s$  is the position of  $s$ -th particle), respectively.  $W(t)$  is a SPH kernel, which is defined as

$$W(t) \equiv \frac{1}{\pi} \begin{cases} 1 - (3/2)t^2 + (3/4)t^3 & \text{if } 0 \leq t \leq 1 \\ (2-t)^3/4 & \text{if } 1 \leq t \leq 2 \\ 0 & \text{otherwise.} \end{cases}$$

We assume the specific heat ratio  $\gamma = 5/3$ , the mean molecular mass  $\mu = 0.5$ , the proton mass  $m_p = 1.6726231 \times 10^{-24} [g]$ . The smoothing length of a SPH particle is calculated in the usual way of SPH method.

In order to obtain smoothed dark matter distribution, we adopt a SPH like method for dark matter particles. The smoothing length of each dark matter particle is determined by

$$h^{(n)} = \frac{1}{2} \left\{ 1 + \left( \frac{n_s}{N^{(n-1)}} \right)^{1/3} \right\} h^{(n-1)}, \quad (3)$$

where the superscript,  $n$ , means  $n$ -th step's value in our iteration method. We set  $n_s = 32$ , and  $h^{(0)} = 1.0 \times 10^{-2} Mpc$ . The calculation is iterated until the neighbor particle number  $N^{(n)}$  (the number of particles inside of a sphere of radius  $h^{(n)}$ ) becomes  $32 \pm 3$ .

At a grid point  $\mathbf{r}_{ij}$  on the  $xy$ -plane, the column density,  $\sigma$ , and the X-ray surface brightness,  $\Sigma_X$ , are calculated from density and temperature at the 3D grid points as follows.

$$\sigma(\mathbf{r}_{ij}) = \sum_k \{\rho_{\text{dm}}(\mathbf{r}_{ijk}) + \rho_{\text{gas}}(\mathbf{r}_{ijk})\} \Delta x \quad (4)$$

and

$$\Sigma_X(\mathbf{r}_{ij}) = \sum_k \Lambda_X \rho_{\text{gas}}^2(\mathbf{r}_{ijk}) T^{1/2}(\mathbf{r}_{ijk}) \Delta x, \quad (5)$$

where  $\Delta x$  is the interval of grids.  $\Lambda_X$  is the coefficient in the formula of X-ray emissivity. In this paper, since we concern only cluster's shape, we assume  $\Lambda_X$  unity. We also calculate  $\sigma$  and  $\Sigma_X$  on the  $yz$ - and the  $zx$ -plane in the same way.

Model	z=0	z=0.5
$\Lambda$ CDM	10.2%	3.64%
OCDM	11.4%	5.21%

Table 2: The ratios of the mass involved in the clusters to total mass in simulations.

## 2.4. Statistical Indicator

We calculate statistical indicators for each cluster of galaxies to quantify its substructure and perform the KS-test. As statistical indicators, we use the axial ratio, the  $M_{\text{int}}$ , the multipole moment power ratio, and the center shift. Definitions of them are described below.

### 2.4.1. Axial Ratio

Axial ratio is a indicator to show the deviation from sphericity of clusters of galaxies (Thomas et al. 1998). On the coordinate whose origin is at center of a cluster, following tensor's eigenvalues are calculated.

$$I_{ij} = \sum mx_i x_j. \quad (6)$$

These eigenvalues are labeled  $\lambda_1, \lambda_2, \lambda_3$  in decreasing order. If clusters are ellipsoid, its axial ratio is obtained by  $(\lambda_1/\lambda_3)^{1/2}$ .

### 2.4.2. $M_{\text{int}}$

We calculate  $M_{\text{int}}$  in a similar way to Thomas et al. (1998). For each cluster we perform Friends-of-Friends and then gradually decrease the linking length,  $l$ . This causes the cluster to break up into subclumps.  $M_{\text{int}}$  is defined as

$$M_{\text{int}} = \frac{m_1 + m_2 + m_3}{m_1}, \quad (7)$$

where  $m_1 \geq m_2 \geq m_3$  are the masses of the three largest clumps. The initial value of  $l$  is  $\bar{n}_c^{-1/3}$ , where  $\bar{n}_c$  is mean number density of dark matter particles and SPH particles in the cluster, and then  $l$  is lowered by a factor of  $100^{1/3}$ . Since  $M_{\text{int}}$  depends on  $l$ , the maximum value of  $M_{\text{int}}$  is used as a measure of clumpiness of the cluster.

### 2.4.3. Center Shift

We calculate the center shift for each cluster in a slightly different way to Jing et al. (1995). We first pick up a peak value,  $c_{\text{peak}}$ , of projected  $\sigma$  or  $\Sigma_X$  of the cluster. Then the lowest contour level,  $c_{\text{lowest}}$ , is defined by the mean value at  $0.5r_{200}$ . And then the  $i$ -th

contour level is determined as  $c_i \equiv c_{\text{peak}}(c_{\text{lowest}}/c_{\text{peak}})^{i/n}$ , where  $n$  is the total number of contours. For the larger  $n$ , the intervals of contour levels become smaller.

The center shift,  $C$ , is defined as

$$C = \sum_{i=1}^n w_i \{(x_i - \bar{x})^2 + (y_i - \bar{y})^2\}, \quad (8)$$

where  $(x_i, y_i)$  is the center of  $i$ th contour, and  $\bar{x} = \sum_i w_i x_i$ , and  $\bar{y} = \sum_i w_i y_i$ . The weight of each contour,  $w_i$ , is proportional to the surface integral of  $\sigma$  or  $\Sigma_X$  in a region between this contour and the adjacent outer contour. The center shift shows emission-weighted dispersion of the centers of contours. If a cluster has a substructure, outer contour's center is expected to shift from  $(\bar{x}, \bar{y})$  and the center shift becomes large.

#### 2.4.4. Power Ratio

The power ratios quantify the shape of projected cluster's potentials and are derived from its multipole expansion(e.g. Buote & Tsai 1995; Buote 1998; Valdarnini, Ghissardi, & Bonometto 1999).

Two-dimensional potential,  $\Psi(R, \phi)$ , and column density,  $\sigma(R, \phi)$ , are related by Poisson equation,

$$\nabla^2 \Psi(R, \phi) = \sigma(R, \phi), \quad (9)$$

where  $R$  and  $\phi$  are a projected polar coordinate about the cluster center, and we here ignore constant factor. Multipole expansion of  $\Psi(R, \phi)$  which relies on the interior material of  $R_{ap}$  (e.g. Buote & Tsai 1995) is

$$\begin{aligned} \Psi(R_{ap}, \phi') = & -a_0 \ln \left( \frac{1}{R_{ap}} \right) - \sum_{m=1}^{\infty} \frac{1}{m R_{ap}^m} \\ & \times (a_m \cos m\phi' + b_m \sin m\phi'), \end{aligned} \quad (10)$$

where  $a_m$  and  $b_m$  are defined as follows.

$$a_m = \int_{R \leq R_{ap}} \sigma(R, \phi) R^m \cos m\phi \, d^2x \quad (11)$$

and

$$b_m = \int_{R \leq R_{ap}} \sigma(R, \phi) R^m \sin m\phi \, d^2x. \quad (12)$$

The  $m$ -th moment power,  $P_m(R_{ap})$ , is defined by integration of squared  $m$ -th term of  $\Psi(R, \phi)$  over the boundary of a circular aperture of radius  $R_{ap}$ .

$$P_m(R_{ap}) = \frac{1}{2m^2 R_{ap}^{2m}} (a_m^2 + b_m^2) \quad (13)$$

for  $m > 0$  and

$$P_0 = a_0^2 \quad (14)$$

for  $m = 0$ .

The moment power depends on not only the irregularity of the potential shape, but also the magnitude of  $\sigma$ . Thus we use the moment power ratio,  $P_m/P_0$ , as an indicator of cluster's substructure. We define the unit of  $R$ , radius of polar coordinate, as  $r_{200}$ , so that the power ratio to be independent of the size of the cluster. Since the origin of polar coordinate is the center, the dipole moment,  $P_1$ , is vanished. Since the higher order ( $m > 4$ , in this paper) terms are affected by minor irregularity of cluster shape, we use power ratio for only  $m = 2, 3$ , and  $4$ .

We also use the same definition of the power ratio for  $\Sigma_X$  in stead of  $\sigma$  in equations (11) and (12).

### 3. RESULT

According to the analytical results by Richstone, Loeb, & Turner (1992), the formation epoch of the galaxy clusters in  $\Lambda$ CDM delays to later epoch than in OCDM. This delay clearly appears in low- $z$  ( $z \lesssim 0.8$ –0.7, as shown in Fig.1). Then we calculate indicators described in §2 at  $z = 0$  and  $z = 0.5$  and perform the KS-test for each set of indicators calculated for two cosmological models,  $\Lambda$ CDM and OCDM. The KS-test can be used as a statistical test to estimate the ability of a indicator to be used to distinguish between the two models. The result of the KS-test is the probability of null-hypothesis that two distributions of the indicator are generated from the same population (Press et al. 1988). The significant level of the KS-test adopted in this paper is 5%. If the result of the KS-test for a indicator is under this level, we can distinguish two cosmological models by using this indicator.

#### 3.1. Axial Ratio

The mean value of the axial ratio is shown in Table 3. From  $z = 0.5$  to  $z = 0$  the axial ratio decreases as the clusters relax. At  $z = 0$ , the axial ratio in  $\Lambda$ CDM is larger than

in OCDM. From analytical prediction (Richstone, Loeb, & Turner 1992), cluster formation delays in  $\Lambda$ CDM. Recent formation of cluster means that fraction of clusters having irregular structures becomes large, thus larger axial ratio in  $\Lambda$ CDM is consistent with the prediction.

The results of the KS-test for axial ratio are 0.495 for  $z = 0$ , and 0.661 for  $z = 0.5$ . Both are over the significant level(5%). Then the axial ratio is not useful to distinguish these two cosmological models.

### 3.2. $M_{\text{int}}$

The mean values of  $M_{\text{int}}$  are shown in Table 4. Similar to the axial ratio  $M_{\text{int}}$  in  $\Lambda$ CDM is larger than that in OCDM at  $z = 0$ .

The results of the KS-test for  $M_{\text{int}}$  are 0.770 for  $z = 0$  and 0.192 for  $z = 0.5$ . Both of them are over the significant level. In this case, we can not use this indicator to distinguish between these two cosmological models again.

### 3.3. Center Shift

The mean values and the standard deviations of logarithm of the center shifts are shown in Table 5. The number of the contours,  $n_{\text{cont}}$ , is varied from 4 to 8 to investigate effect of the number of the contours. For large  $n$ , i.e. a small interval of contour level,  $C$  is large. In the case of a small interval, the center shift is easy to reflect small substructure nearby the center of the cluster.

The center shifts for  $\sigma$ ,  $C_\sigma$ , are significantly larger than those for  $\Sigma_X$ ,  $C_{\Sigma_X}$ . The shapes of the  $\Sigma_X$  contours reflect the distribution of the gas and gas in the cluster relaxes more quickly than the collisionless dark matter (Frenk et al. 1999). This is the reason why the shapes of  $\Sigma_X$  contour become rounder than those of  $\sigma$  and the center shifts for  $\Sigma_X$  become smaller more quickly than those for  $\sigma$ .

redshift	$\Lambda$ CDM	OCDM
$z = 0$	1.608	1.585
$z = 0.5$	1.644	1.696

Table 3: The mean value of the axial ratio.

redshift	$\Lambda$ CDM	OCDM
$z = 0$	1.289	1.188
$z = 0.5$	1.284	1.189

Table 4: The mean value of the  $M_{\text{int}}$ .

Model	$n_{\text{cont}}$	$\log(C_\sigma)$	$\log(C_{\Sigma_X})$
$\Lambda$ CDM			
$(z = 0)$	4	$-2.65(\pm 0.72)$	$-3.43(\pm 0.78)$
	5	$-2.52(\pm 0.69)$	$-3.31(\pm 0.82)$
	6	$-2.43(\pm 0.67)$	$-3.26(\pm 0.80)$
	7	$-2.38(\pm 0.64)$	$-3.22(\pm 0.80)$
	8	$-2.33(\pm 0.63)$	$-3.20(\pm 0.77)$
OCDM			
$(z = 0)$	4	$-2.80(\pm 0.70)$	$-3.64(\pm 0.75)$
	5	$-2.72(\pm 0.66)$	$-3.56(\pm 0.77)$
	6	$-2.62(\pm 0.67)$	$-3.49(\pm 0.75)$
	7	$-2.59(\pm 0.63)$	$-3.47(\pm 0.76)$
	8	$-2.54(\pm 0.62)$	$-3.46(\pm 0.76)$
$\Lambda$ CDM			
$(z = 0.5)$	4	$-2.87(\pm 0.58)$	$-3.73(\pm 0.67)$
	5	$-2.71(\pm 0.60)$	$-3.62(\pm 0.64)$
	6	$-2.67(\pm 0.57)$	$-3.53(\pm 0.64)$
	7	$-2.63(\pm 0.55)$	$-3.49(\pm 0.67)$
	8	$-2.59(\pm 0.55)$	$-3.45(\pm 0.64)$
OCDM			
$(z = 0.5)$	4	$-2.99(\pm 0.68)$	$-3.68(\pm 0.77)$
	5	$-2.89(\pm 0.70)$	$-3.59(\pm 0.80)$
	6	$-2.77(\pm 0.68)$	$-3.53(\pm 0.76)$
	7	$-2.73(\pm 0.70)$	$-3.46(\pm 0.76)$
	8	$-2.68(\pm 0.69)$	$-3.41(\pm 0.80)$

Table 5: Mean value of logarithm of center shifts

Note. — First column indicates cosmological model and redshift. Second column shows the number of contours. Third and forth columns are mean value of  $\log(C)$  for the column density and the X-ray surface brightness, respectively.

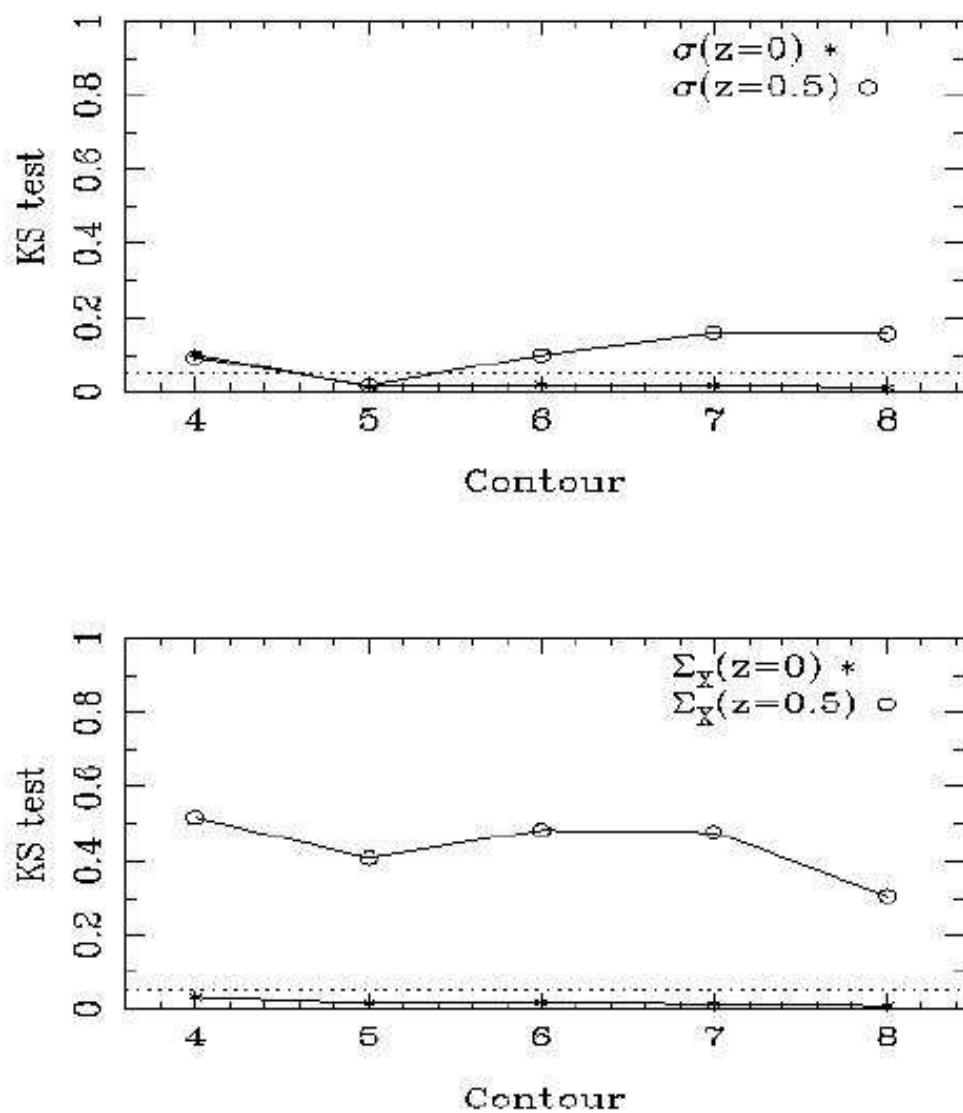


Fig. 2.— The result of the KS-test for center shifts as a function of the number of contours. Asterisks indicate the results at  $z = 0$ , and circles indicate the results at  $z = 0.5$ . Dotted line describes the significant level(5%)

The center shifts in  $\Lambda$ CDM are larger than those in OCDM at the same redshift. This results reflects that the formation epoch of the clusters in  $\Lambda$ CDM is in later than in OCDM.

Fig.2 is the result of the KS-test for the center shifts. The upper panel describes the results for the center shifts for the column density and the lower one describes the results for the X-ray surface brightness. Dotted line indicates the significant level(5%). Asterisks indicate the results at  $z = 0$ , and circles indicate the results at  $z = 0.5$ . Using the center shifts for  $\Sigma_X$  at  $z = 0$ , we can distinguish two cosmological models in this range of number of contours. The effect of contour level interval is not so significant for the KS-test.

In order to estimate the effect of the lowest level of contour, we also calculate the center shift for  $\Sigma_X$  and  $\sigma$  in the two cases in which the lowest contour level is the mean value at  $0.4r_{200}$  and  $0.7r_{200}$ . For the case of  $0.7r_{200}$ , the results of the KS-test are over the significant level, except for only one case of  $C_{\Sigma_X}$  ( $z=0$ ,  $n_{\text{cont}} = 8$ ). For the case of  $0.4r_{200}$ , the results are similar to the case of the lowest level is  $0.5r_{200}$ . We conclude that the center shift inside of  $\sim 0.5r_{200}$  is useful tool to clarify the presence of cosmological constant.

### 3.4. Power Ratio

We calculate the power ratios for various  $R_{ap}$ , that is, 0.4, 0.5, 0.6, 0.8, and 1.0 times  $r_{200}$ , in order to show how  $R_{ap}$  affects the result of the KS-test. We show the mean values and the standard deviations of logarithm of the power ratio in Table 6 and 7, for the column density and the X-ray surface brightness, respectively. For small  $R_{ap}$ , the power ratios are large. The most likely explanation of this property is that the power ratios for small  $R_{ap}$  are easy to reflect the small size substructure nearby the center of the cluster.

From  $z = 0.5$  to  $z = 0$  the power ratios become smaller in both models. This is due to the fact that fraction of relaxed clusters increases with time. Similar to the other indicators, the power ratios in  $\Lambda$ CDM are larger than those in OCDM at the same redshift. This is explained by the fact that galaxy cluster formation proceeds in later epoch in  $\Lambda$ CDM than in OCDM as shown in Fig.1.

Table 8 shows the results of the KS-test for the power ratio for the column density, and Table 9 shows those for the X-ray surface brightness. The results with asterisk in these tables mean that they are under the level of significance (5%). Figure 3–5 show the results of the KS-tests summarized in Table 8 and 9. At  $z = 0$ , we can distinguish two cosmological models by the power ratios for  $\Sigma_X$  for all  $R_{ap}$ . Using the power ratios for  $\sigma$  for most  $R_{ap}$ , except for  $P_3/P_0$ , we can also distinguish two cosmological models.

Model	$R_{ap}$	$\log(P_2/P_0)$	$\log(P_3/P_0)$	$\log(P_4/P_0)$
$\Lambda$ CDM				
( $z = 0$ )	$0.4r_{200}$	$-2.90(\pm 0.66)$	$-4.38(\pm 0.69)$	$-4.89(\pm 0.75)$
	$0.5r_{200}$	$-2.94(\pm 0.63)$	$-4.52(\pm 0.71)$	$-4.91(\pm 0.66)$
	$0.6r_{200}$	$-2.98(\pm 0.61)$	$-4.61(\pm 0.68)$	$-4.96(\pm 0.66)$
	$0.8r_{200}$	$-3.05(\pm 0.66)$	$-4.63(\pm 0.69)$	$-5.05(\pm 0.72)$
	$1.0r_{200}$	$-3.15(\pm 0.68)$	$-4.70(\pm 0.67)$	$-5.20(\pm 0.74)$
OCDM				
( $z = 0$ )	$0.4r_{200}$	$-3.03(\pm 0.63)$	$-4.58(\pm 0.79)$	$-5.11(\pm 0.81)$
	$0.5r_{200}$	$-3.09(\pm 0.68)$	$-4.63(\pm 0.74)$	$-5.11(\pm 0.80)$
	$0.6r_{200}$	$-3.15(\pm 0.76)$	$-4.61(\pm 0.76)$	$-5.10(\pm 0.84)$
	$0.8r_{200}$	$-3.20(\pm 0.65)$	$-4.72(\pm 0.75)$	$-5.22(\pm 0.80)$
	$1.0r_{200}$	$-3.29(\pm 0.65)$	$-4.85(\pm 0.79)$	$-5.36(\pm 0.76)$
$\Lambda$ CDM				
( $z = 0.5$ )	$0.4r_{200}$	$-2.93(\pm 0.69)$	$-4.33(\pm 0.67)$	$-4.88(\pm 0.69)$
	$0.5r_{200}$	$-2.92(\pm 0.51)$	$-4.37(\pm 0.58)$	$-4.89(\pm 0.65)$
	$0.6r_{200}$	$-2.92(\pm 0.50)$	$-4.40(\pm 0.57)$	$-4.85(\pm 0.66)$
	$0.8r_{200}$	$-2.91(\pm 0.51)$	$-4.35(\pm 0.51)$	$-4.85(\pm 0.67)$
	$1.0r_{200}$	$-2.93(\pm 0.51)$	$-4.39(\pm 0.63)$	$-4.81(\pm 0.64)$
OCDM				
( $z = 0.5$ )	$0.4r_{200}$	$-2.76(\pm 0.52)$	$-4.29(\pm 0.93)$	$-4.78(\pm 0.86)$
	$0.5r_{200}$	$-2.78(\pm 0.52)$	$-4.38(\pm 0.93)$	$-4.75(\pm 0.80)$
	$0.6r_{200}$	$-2.80(\pm 0.54)$	$-4.40(\pm 0.90)$	$-4.79(\pm 0.82)$
	$0.8r_{200}$	$-2.87(\pm 0.61)$	$-4.43(\pm 0.77)$	$-4.90(\pm 0.96)$
	$1.0r_{200}$	$-3.02(\pm 0.64)$	$-4.44(\pm 0.73)$	$-5.02(\pm 0.94)$

Table 6: Mean value of  $\log(P_m/P_0)$  for column density

Note. — First column describes cosmological models and redshifts. Upper two blocks are the data at  $z = 0$  and lower two blocks are at  $z = 0.5$ . Second column is aperture radius. From third to fifth columns are mean values of power ratios of second, third, forth order, respectively.

Model	$R_{ap}$	$\log(P_2/P_0)$	$\log(P_3/P_0)$	$\log(P_4/P_0)$
$\Lambda$ CDM				
( $z = 0$ )	$0.4r_{200}$	$-3.92(\pm 0.96)$	$-5.86(\pm 1.14)$	$-6.52(\pm 1.31)$
	$0.5r_{200}$	$-4.19(\pm 0.99)$	$-6.16(\pm 1.14)$	$-6.81(\pm 1.32)$
	$0.6r_{200}$	$-4.40(\pm 1.01)$	$-6.36(\pm 1.22)$	$-7.03(\pm 1.34)$
	$0.8r_{200}$	$-4.75(\pm 1.05)$	$-6.66(\pm 1.32)$	$-7.37(\pm 1.41)$
	$1.0r_{200}$	$-5.04(\pm 1.09)$	$-6.93(\pm 1.40)$	$-7.67(\pm 1.49)$
OCDM				
( $z = 0$ )	$0.4r_{200}$	$-4.40(\pm 0.97)$	$-6.45(\pm 1.29)$	$-7.04(\pm 1.42)$
	$0.5r_{200}$	$-4.68(\pm 1.03)$	$-6.70(\pm 1.39)$	$-7.37(\pm 1.59)$
	$0.6r_{200}$	$-4.90(\pm 1.05)$	$-6.83(\pm 1.40)$	$-7.51(\pm 1.58)$
	$0.8r_{200}$	$-5.23(\pm 1.12)$	$-7.11(\pm 1.55)$	$-7.84(\pm 1.70)$
	$1.0r_{200}$	$-5.52(\pm 1.15)$	$-7.38(\pm 1.60)$	$-8.19(\pm 1.76)$
$\Lambda$ CDM				
( $z = 0.5$ )	$0.4r_{200}$	$-3.54(\pm 0.83)$	$-5.41(\pm 1.08)$	$-5.99(\pm 1.10)$
	$0.5r_{200}$	$-3.79(\pm 0.90)$	$-5.64(\pm 1.07)$	$-6.30(\pm 1.15)$
	$0.6r_{200}$	$-3.97(\pm 0.90)$	$-5.79(\pm 1.03)$	$-6.50(\pm 1.21)$
	$0.8r_{200}$	$-4.28(\pm 0.97)$	$-6.04(\pm 1.05)$	$-6.74(\pm 1.28)$
	$1.0r_{200}$	$-4.50(\pm 1.11)$	$-6.08(\pm 1.31)$	$-6.76(\pm 1.49)$
OCDM				
( $z = 0.5$ )	$0.4r_{200}$	$-3.63(\pm 1.16)$	$-5.35(\pm 1.53)$	$-6.03(\pm 1.64)$
	$0.5r_{200}$	$-3.87(\pm 1.20)$	$-5.59(\pm 1.59)$	$-6.26(\pm 1.75)$
	$0.6r_{200}$	$-4.04(\pm 1.21)$	$-5.83(\pm 1.66)$	$-6.45(\pm 1.79)$
	$0.8r_{200}$	$-4.29(\pm 1.35)$	$-6.05(\pm 1.77)$	$-6.71(\pm 2.05)$
	$1.0r_{200}$	$-4.59(\pm 1.40)$	$-6.30(\pm 1.87)$	$-6.98(\pm 2.08)$

Table 7: Mean value of  $\log(P_m/P_0)$  for X-ray surface brightness

---

Note. — Each columns mean similar to Table 6

$P_m/P_0$	$R_{ap}$	$z = 0$	$z = 0.5$
$P_2/P_0$			
$0.4r_{200}$	2.43e-02*	4.45e-01	
$0.5r_{200}$	9.03e-02	4.57e-01	
$0.6r_{200}$	3.30e-02*	3.21e-01	
$0.8r_{200}$	1.38e-02*	6.84e-01	
$1.0r_{200}$	5.79e-03*	1.04e-01	
$P_3/P_0$			
$0.4r_{200}$	4.38e-02*	1.16e-01	
$0.5r_{200}$	1.23e-01	2.20e-01	
$0.6r_{200}$	3.37e-01	8.40e-02	
$0.8r_{200}$	4.28e-02*	4.87e-02*	
$1.0r_{200}$	1.24e-01	2.32e-01	
$P_4/P_0$			
$0.4r_{200}$	3.25e-02*	4.25e-01	
$0.5r_{200}$	1.40e-03*	3.60e-01	
$0.6r_{200}$	1.53e-02*	2.81e-01	
$0.8r_{200}$	1.43e-02*	1.36e-01	
$1.0r_{200}$	8.48e-02	8.97e-02	

Table 8: The results of the KS-test for power ratio for the column density.

$P_m/P_0$	$R_{ap}$	$z = 0$	$z = 0.5$
$P_2/P_0$			
$0.4r_{200}$	4.19e-08*	1.03e-02*	
$0.5r_{200}$	7.20e-08*	1.47e-02*	
$0.6r_{200}$	1.33e-06*	2.70e-02*	
$0.8r_{200}$	1.47e-06*	2.99e-02*	
$1.0r_{200}$	2.56e-06*	3.30e-02*	
$P_3/P_0$			
$0.4r_{200}$	6.75e-06*	2.12e-01	
$0.5r_{200}$	3.51e-05*	1.42e-01	
$0.6r_{200}$	4.43e-05*	9.17e-03*	
$0.8r_{200}$	2.24e-03*	1.15e-03*	
$1.0r_{200}$	7.99e-04*	2.43e-03*	
$P_4/P_0$			
$0.4r_{200}$	2.06e-06*	1.79e-01	
$0.5r_{200}$	6.83e-05*	9.77e-02	
$0.6r_{200}$	4.72e-05*	3.22e-02*	
$0.8r_{200}$	2.52e-04*	1.28e-02*	
$1.0r_{200}$	7.56e-05*	2.68e-03*	

Table 9: The results of the KS-test for power ratio for the X-ray surface brightness.

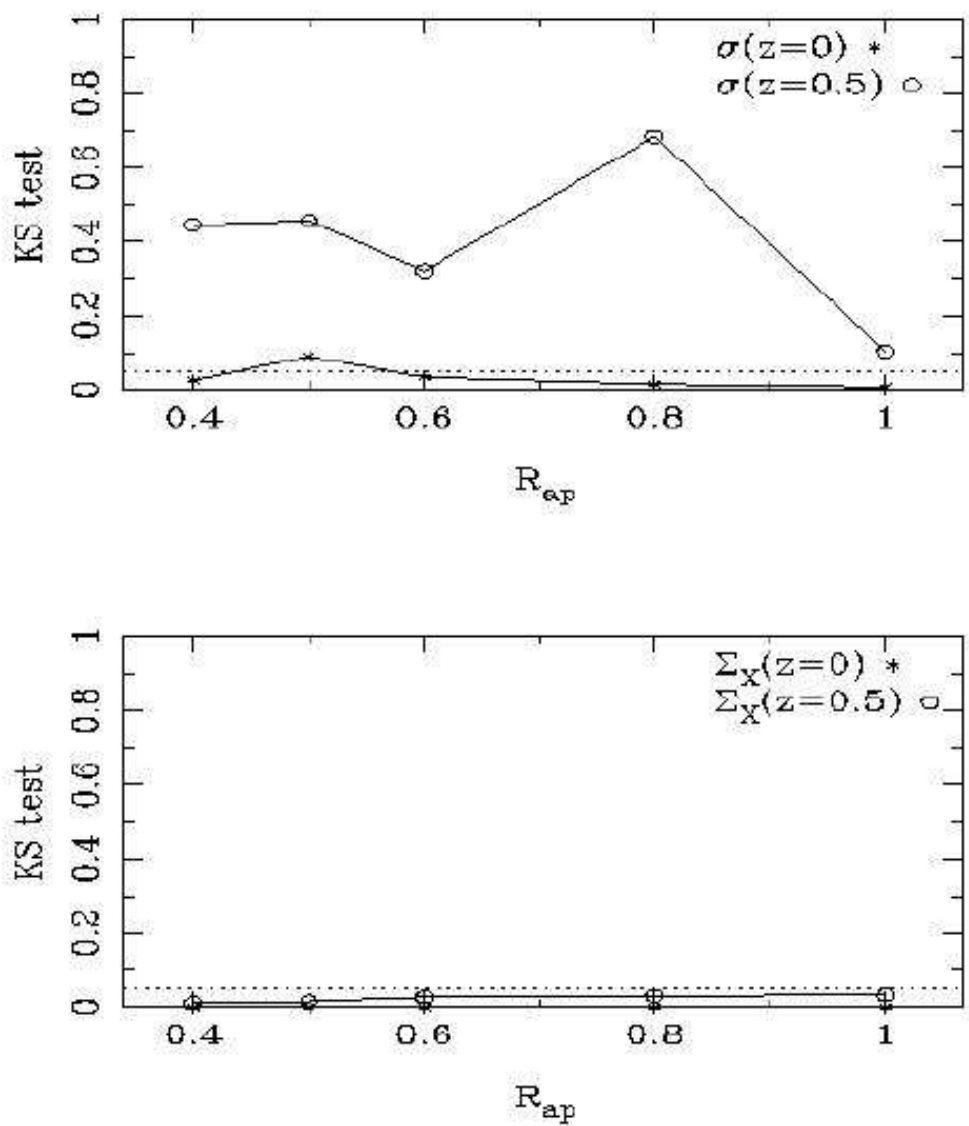


Fig. 3.— The results of the KS-test for  $P_2/P_0$ . Asterisks indicate the results at  $z = 0$ , and circles indicate the results at  $z = 0.5$ . Dotted line indicates the significant level(5%)

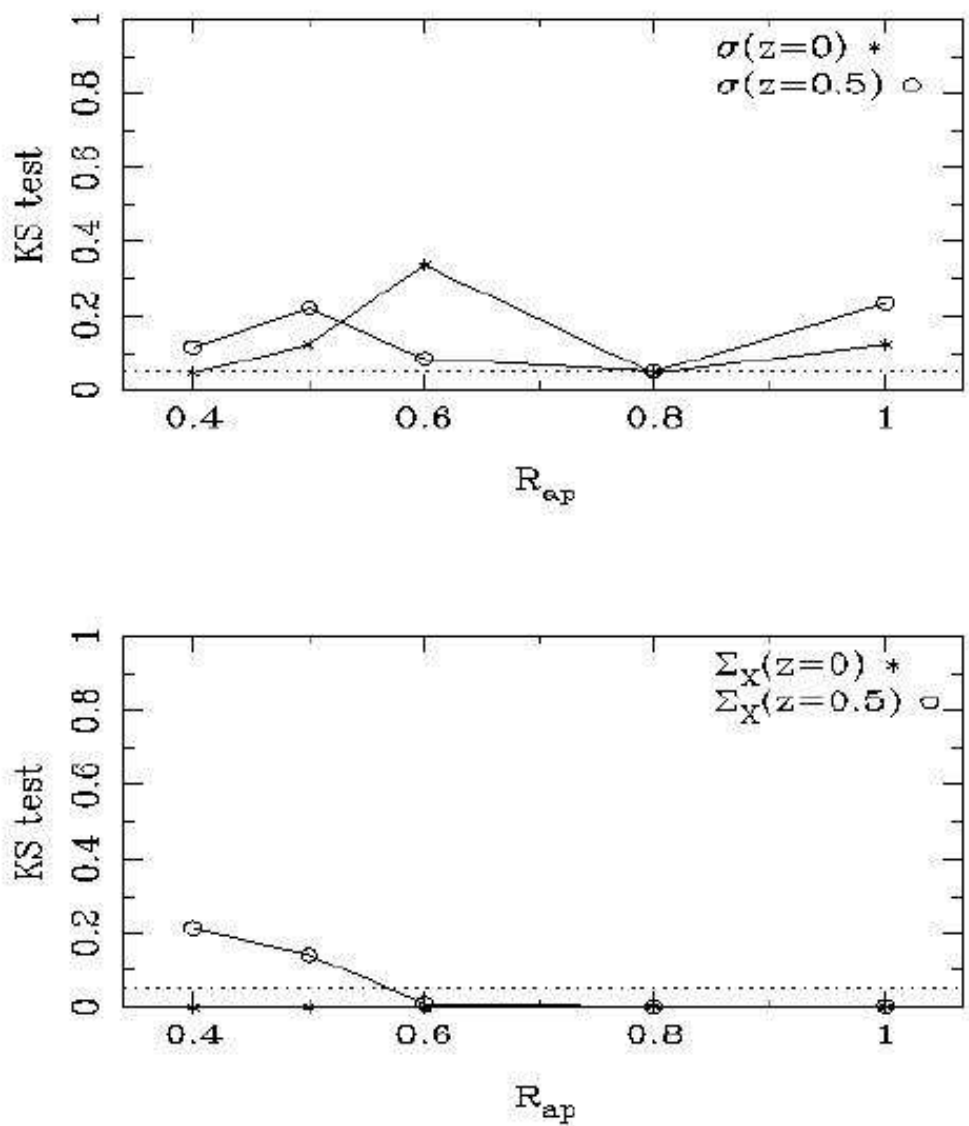


Fig. 4.— The results of the KS-test for  $P_3/P_0$ . Asterisks indicate the results at  $z = 0$ , and circles indicate the results at  $z = 0.5$ . Dotted line indicates the significant level(5%)

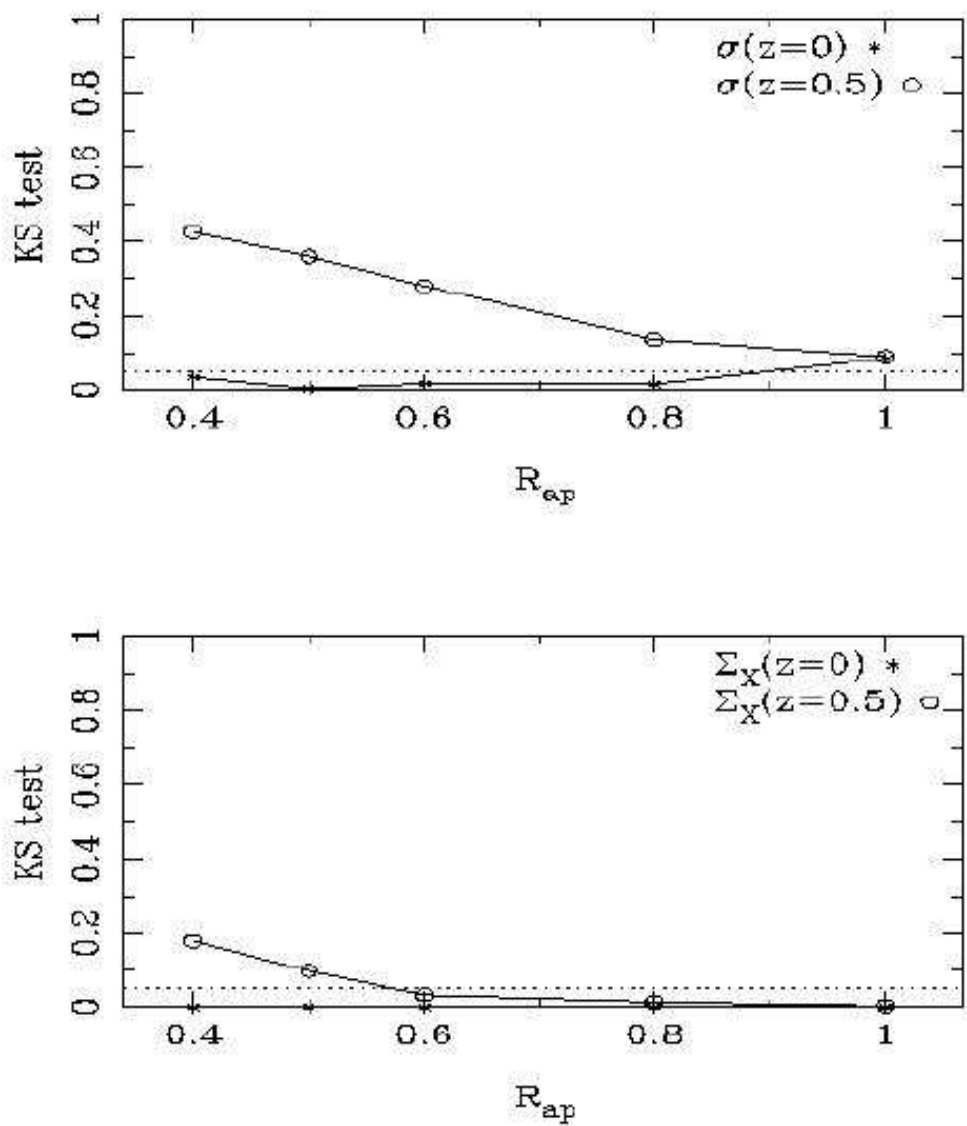


Fig. 5.— The results of the KS-test for  $P_4/P_0$ . Asterisks indicate the results at  $z = 0$ , and circles indicate the results at  $z = 0.5$ . Dotted line indicates the significant level(5%)

It is difficult to get the power ratios of observed clusters for same  $R_{ap}$  in the unit of  $r_{200}$ , e.g.  $R_{ap} = 0.4r_{200}$ . In order to estimate the effect of variation of observed  $R_{ap}$ , we calculate the power ratios for  $\Sigma_X$  and  $\sigma$  for  $R_{ap}$  with a variation. We assume the Gaussian distribution of  $R_{ap}$  with the mean value of  $0.4r_{200}$  and its variation of  $0.1\text{--}0.2r_{200}$  for clusters in our numerical results. The probability in  $r < R_{ap} < r + dr$  is

$$P(r < R_{ap} < r + dr) \propto \exp[(0.4r_{200} - r)^2/s^2] dr,$$

where  $s = 0.1r_{200}$  or  $0.2r_{200}$ . In Table 10, we show the results of the KS-test for the power ratios calculated for the Gaussian distribution of  $R_{ap}$ , and those for  $R_{ap} = 0.4r_{200}$ , which are already obtained. For  $\Sigma_X$ , the results of the KS-test for the different cosmological models are lower than the significant level (5%) and those for the same model are higher than the significant level. This indicates that comparison of power ratio between simulated clusters and observed data is a useful tool to distinguish between  $\Lambda$ CDM and OCDM if the standard deviation of observed  $R_{ap}$  is less than  $0.2r_{200}$ . For  $\sigma$ , however, the results of the KS-test for different cosmological models are higher than the significant level even if the standard deviation of  $R_{ap}$  is as large as  $0.1r_{200}$ , except for  $P_4/P_0(0.4r_{200})$  in OCDM as shown in Table 10. The power ratio of observed clusters for  $\sigma$  should be calculated for the observed data with small variation of  $R_{ap}$  of which the standard deviation is less than  $0.1r_{200}$ .

#### 4. DISCUSSION AND CONCLUSION

We have examined the substructure of the simulated galaxy clusters in two different cosmological models,  $\Lambda$ CDM and OCDM, at  $z = 0$  and  $z = 0.5$ . For each cluster we have calculated the axial ratio,  $M_{\text{int}}$ , the center shift, and the multipole moment power ratio as statistical indicators which quantify substructure of clusters. At  $z = 0$  all of mean values of these indicators in  $\Lambda$ CDM show larger values than those in OCDM. These large values of the indicators, which mean large irregularity of clusters, implies a recent formation of the cluster. This can be explained by the fact that the typical formation epoch of galaxy clusters in  $\Lambda$ CDM is later than in OCDM and a cluster which is formed in later epoch is expected to have more irregular structure now (Richstone, Loeb, & Turner 1992). Our results are consistent with this analytical prediction and other previous numerical studies (Mohr et al. 1995; Crone, Evrard, & Richstone 1996; Buote & Xu 1997).

The power ratio and the center shift are calculated for X-ray surface brightness ( $\Sigma_X$ ) and column density ( $\sigma$ ) distributions of clusters. Both of the indicators for  $\sigma$  show larger value than those for  $\Sigma_X$ . This implies that the dark matter distribution of a cluster, which dominates the structure of  $\sigma$ , is harder to relax than the gas distribution which is closely related with the structure of  $\Sigma_X$  (Frenk et al. 1999).

	$(0.4 \pm 0.1)r_{200}$ ( $\Lambda$ CDM)	$(0.4 \pm 0.2)r_{200}$ ( $\Lambda$ CDM)	$(0.4 \pm 0.1)r_{200}$ (OCDM)	$(0.4 \pm 0.2)r_{200}$ (OCDM)
$\sigma$				
$P_2/P_0(0.4r_{200})$ ( $\Lambda$ CDM)	9.623e-01	5.376e-01	1.071e-01	2.284e-01
$P_2/P_0(0.4r_{200})$ (OCDM)	7.364e-02	7.577e-02	9.932e-01	6.115e-01
$P_3/P_0(0.4r_{200})$ ( $\Lambda$ CDM)	7.869e-01	8.514e-02	1.524e-01	2.232e-01
$P_3/P_0(0.4r_{200})$ (OCDM)	1.972e-01	3.637e-01	9.019e-01	3.285e-01
$P_4/P_0(0.4r_{200})$ ( $\Lambda$ CDM)	9.200e-01	3.865e-01	2.573e-01	8.110e-01
$P_4/P_0(0.4r_{200})$ (OCDM)	7.898e-03*	2.744e-02*	1.197e-01	9.518e-02
$\Sigma_X$				
$P_2/P_0(0.4r_{200})$ ( $\Lambda$ CDM)	9.623e-01	7.869e-01	1.142e-06*	6.748e-05*
$P_2/P_0(0.4r_{200})$ (OCDM)	3.488e-08*	7.199e-08*	6.914e-01	1.197e-01
$P_3/P_0(0.4r_{200})$ ( $\Lambda$ CDM)	7.054e-01	6.208e-01	3.231e-06*	5.578e-05*
$P_3/P_0(0.4r_{200})$ (OCDM)	3.037e-05*	4.006e-06*	9.999e-01	5.331e-01
$P_4/P_0(0.4r_{200})$ ( $\Lambda$ CDM)	9.970e-01	3.865e-01	6.945e-06*	3.667e-04*
$P_4/P_0(0.4r_{200})$ (OCDM)	8.322e-06*	4.181e-06*	8.411e-01	6.115e-01

Table 10: KS-test for power ratios for precise and Gaussian distributed  $R_{ap}$

Note. — The results of the KS-test for power ratios calculated for precise  $0.4r_{200}$  and those calculated for Gaussian distributed  $R_{ap}$ . The results with asterisk in these tables mean that they are under the significant level (5%).

We use the KS-test to estimate the ability of the indicators to distinguish between two cosmological models. We can not distinguish two models by the axial ratio and  $M_{\text{int}}$ . Using the center shift and the power ratio for  $\Sigma_X$  at  $z = 0$ , we can distinguish two cosmological models. We can also distinguish two cosmological models by the center shifts,  $P_2/P_0$ , and  $P_4/P_0$  for  $\sigma$  at  $z = 0$ . At  $z = 0.5$  we can distinguish two cosmological models by the power ratio for  $\Sigma_X$ , but can not by the center shift for  $\Sigma_X$  and both the power ratio and the center shift for  $\sigma$ .

Using the power ratios for  $\Sigma_X$  we can distinguish between  $\Lambda\text{CDM}$  and  $\text{OCDM}$  better than using those for  $\sigma$  as shown in Table 8 and 9. One explanation for the difference between the results for  $\Sigma_X$  and  $\sigma$  is that the relaxation time scale of structure for  $\sigma$  is longer than that for  $\Sigma_X$  as described above (Frenk et al. 1999). The structure of dark matter is harder to relax than that of gas, hence the indicators for  $\sigma$ , which reflects the distribution of dark matter, remains a large value after the formation of cluster. Since the power ratios for  $\sigma$  tend to show the trail of early formation of clusters as described above, it is not adequate to distinguish between two cosmological models by the power ratios for  $\sigma$ .

Another possible reason for the difference is that the power ratios for  $\Sigma_X$  mainly depend on higher density region than those for  $\sigma$ , since  $\Sigma_X$  is proportional to square of gas density (and square root of temperature,  $\rho_{\text{gas}}^2 T^{1/2}$ ). This suggests that it is suitable to focus on structure at the central region to distinguish between  $\Lambda\text{CDM}$  and  $\text{OCDM}$ .

Some previous studies compare  $\Lambda\text{CDM}$  and  $\text{OCDM}$  by using only N-body simulations (Jing et al. 1995; Crone, Evrard, & Richstone 1996; Buote & Xu 1997), and they assume that the X-ray emissivity is proportional to  $\rho_{\text{dm}}^2$ . The structure of gas of clusters does not trace the structure of dark matter in the cluster which is not relaxed. We show that the numerical simulations including both dark matter component and gas component are very important by studying the substructure of the clusters by the X-ray surface brightness calculated from the gas distribution.

Although Other study (Mohr et al. 1995) employs gas particle, the number of sample cluster is small (8 clusters for each model). We use the data of so large size simulation ( $L_{\text{box}} = 150h^{-1}\text{Mpc}$ ) that we can obtain a number of clusters enough to perform statistical test (70–80 clusters at  $z=0$ ). The KS-test is significant when the number of samples  $\gtrsim 20$  (Press et al. 1988).

We conclude that the power ratios and the center shifts for  $\Sigma_X$  can be used to distinguish between  $\Lambda\text{CDM}$  and  $\text{OCDM}$  more clearly at  $z = 0$  rather than  $z = 0.5$ .

We thank Professor Masayuki Fujimoto, Takayuki Saitoh, and Yu Moritomo for help-

ful advice, insightful discussions and encouragement. Numerical computation in this work was carried out on the SGI Origin 2000 at the Division of Physics, Graduate School of Science, Hokkaido University, and on the VPP300/16R and VX/4R at the Astronomical Data Analysis Center of National Astronomical Observatory, Japan.

## REFERENCES

Bahcall, N.A., Ostriker, J.P., Perlmutter, S., & Steinhardt, P.J. 1999, *Science*, 284, 1481

Bertschinger, E. 1995, preprint (astro-ph/9506070)

Buote, D.A. 1998, *MNRAS*, 293, 381

Buote, D.A., & Tsai, J.C. 1995b, *ApJ*, 452, 522

Buote, D.A., & Tsai, J.C. 1996, *ApJ*, 458, 27

Buote, D.A., & Xu, G. 1997, *MNRAS*, 284, 439

Clowe, D., Luppino, G.A., Kaiser, N., & Gioia, I.M. 2000, *ApJ*, 539, 540

Crone, M.M., Evrard A.E., & Richstone, D.O. 1996, *ApJ*, 467, 489

de Bernardis, P. et al. 2000, *Nature*, 404, 955

Dutta, S.N. 1995, *MNRAS*, 276, 1109

Frenk, C.S., et al. 1999, *ApJ*, 525, 554

Gibson, B.K., et al. 2000, *ApJ*, 529, 723

Jing, Y.P., & Fang, L.Z. 1994, *ApJ*, 432, 438

Jing, Y.P., Mo, H.J., Börner, G., & Fang, L.Z. 1995, *MNRAS*, 276, 417

Luppino, G.A., & Kaiser, N. 1997, *ApJ*, 475, 20

Mellier, Y. 1999, *ARA&A*, 37, 127

Mohr, J.J., Evrard, A.E., Fabricant, D.G., & Geller, M.J. 1995, *ApJ*, 447, 8

Perlmutter, S., et al. 1999, *ApJ*, 517, 565

Press, W.H., Flannery, B.P., Teukolsky, S.A., & Vetterling, W.T. 1988, *Numerical Recipes in C* (Cambridge: Cambridge Univ. Press)

Richstone, D., Loeb, A., & Turner, E.L. 1992, ApJ, 393, 477

Riess, A.G., et al. 1998, AJ, 116, 1009

Somerville, R.S., & Primack, J.R. 1999, MNRAS, 310, 1087

Thomas, P.A., et al. 1998, MNRAS, 296, 106

Totani, T. & Kobayashi, C. 1999, ApJ, 526, L68

Tsai, J.C., & Buote, D.A. 1996, MNRAS, 282, 77

Valdarnini, R., Ghizzardi, S, & Bonometto, S. 1999, New Astron., 4, 71

Yoshikawa, K., Jing, Y.P., & Suto, Y. 2000, ApJ, 535, 593